ACS APPLIED MATERIALS & INTERFACES

www.acsami.org
Research Article

Overestimation of Operational Stability in Polymer-Based Organic Field-Effect Transistors Caused by Contact Resistance

Kenji Sakamoto,* Takeshi Yasuda, Takeo Minari, Masafumi Yoshio, Junpei Kuwabara, and Masayuki Takeuchi

Cite This: ACS Appl. Mater. Interfaces 2024, 16, 68081−68090
Read Online

ACCESS | Metrics & More | Article Recommendations | Supporting Information

ABSTRACT: The bias-stress effects of bottom-gate top-contact polymer-based organic field-effect transistors (OFETs) with different channel lengths (50−500 μm) were evaluated by repeating cycles of prolonged on-state gate-bias application and transfer characteristics measurements in the linear regime. The thicknesses of poly(didodecylquaterthiophene-*alt*-didodecylbithiazole) active layers were 26 and 37 nm. All OFETs exhibited nonlinear (nonideal) transfer characteristics with a maximum transconductance within the gate-source voltage sweep range. Both a shift in threshold voltage (V_{th}^{lin}) and a reduction in field-effect charge carrier mobility (μ^{lin}) were apparently observed during the bias-stress application. When μ^{lin} and V_{th}^{lin} were conventionally extracted from the transfer characteristics around the maximum transconductance, the V_{th}^{lin} shift amount and μ^{lin} reduction depended on the channel length and were smaller in OFETs with short channels. After contact resistance (R_c) correction, the channel length dependence disappeared. Thus, the operational stability in OFETs with short channels: ≤50 (150) μm for the 26 (37) nm-thick active layers, was found to be overestimated without R_c correction. This erroneous evaluation would become more pronounced in short-channel, high-mobility OFETs, because the R_c becomes larger relative to the channel resistance with increasing μ^{lin} and decreasing channel length. These results suggest that one should pay attention to R_c in the fundamental research into the origin of operational instability and in evaluating the effects of active layers, gate dielectrics, and active layer/gate dielectric interfaces on operational stability.

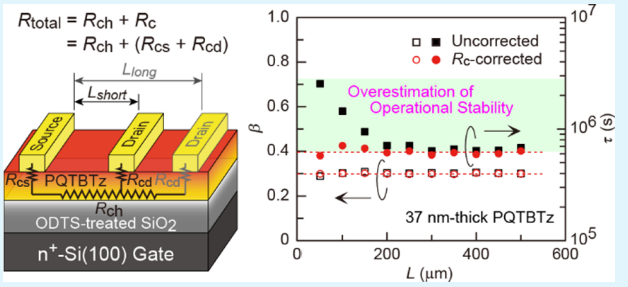

KEYWORDS: *polymer-based organic field-effect transistors, bias-stress effects, contact resistance, modified transmission line method, operational stability*

1. INTRODUCTION

Polymer-based organic field-effect transistors (OFETs) are promising active devices in large-area, low-cost, lightweight, flexible, and stretchable electronics owing to good solution processability and superior mechanical properties of organic semiconducting polymers. Since the cutoff frequency and on-state current of OFETs are proportional to field-effect charge carrier mobility, its improvement is a central issue in OFETs. As a result of enormous efforts since 1986,[1] the field-effect mobility of polymer-based OFETs has been significantly improved,[2] and is now over 10 $cm^2\ V^{-1}\ s^{-1}$.[3−5] (The field-effect mobility of highly oriented poly[4-(4,4-dihexadecyl-4H-cyclopenta[1,2-b:5,4-b']-dithiophen-2-yl)-*alt*-[1,2,5]-thiadiazolo[3,4-*c*]pyridine] (PCDTPT) active layers was overestimated to be >20 $cm^2\ V^{-1}\ s^{-1}$ in ref 4. It was re-estimated to be approximately 10 $cm^2\ V^{-1}\ s^{-1}$ afterward.[6,7]) This significant improvement is due to material synthesis based on a donor−acceptor (D−A) copolymer design concept in which electron-donating and electron-accepting moieties alternate along the backbone structure and development of alignment processes to obtain highly oriented active layers.

Commercial applications of OFETs require long-term operational stability in addition to sufficiently high field-effect mobilities to meet initial specifications. The undesirable change in the electrical characteristics under continuous operation: that is, bias-stress effect, must be minimized. In general, prolonged bias-stress application causes device performance degradation, such as a shift in the threshold voltage, a reduction in the field-effect mobility, an increase in the subthreshold swing, an increase in the off-state current, and/or increased hysteresis in the transfer characteristics.[8,9] In many cases, the operational stability is monitored by the following two methods: (I) repeating cycles of prolonged gate-bias application and transfer characteristics measurement in the linear regime and (II) measuring drain current in the linear

Received: September 12, 2024
Revised: November 13, 2024
Accepted: November 18, 2024
Published: December 1, 2024

https://doi.org/10.1021/acsami.4c15666
ACS Appl. Mater. Interfaces 2024, 16, 68081−68090

regime as a function of time under a constant continuous on-state gate-bias application.[10] Then, to quantify the observed bias-stress effects, the bias-stress time dependence of the threshold voltage shift ($\Delta V_{th}^{lin}(t) = V_{th}^{lin}(t) - V_{th0}^{lin}$) or the on-state drain current ($I_d(t)$) is fitted with the following stretched exponential functions:

$$\Delta V_{th}^{lin}(t) = (V_{gs} - V_{th0}^{lin})\cdot\{1 - \exp[-(\frac{t}{\tau})^{\beta}]\} \quad (1a)$$

and

$$I_d(t) = I_{d0}\cdot\exp[-(\frac{t}{\tau})^{\beta}] \quad (1b)$$

where V_{gs} is the gate-source voltage; V_{th0}^{lin} and I_{d0} are $V_{th}^{lin}(0)$ and $I_d(0)$, respectively; τ is the trapping time constant of carriers to fill trap levels; and β ($0 \le \beta \le 1$) is a stretching factor representing the distribution of time constants.[10,11] τ and β are used to compare the operational stability among different OFETs. Method I has the advantage of determining not only the shift in threshold voltage but also the changes in field-effect mobility, subthreshold swing, off-state current, and transfer curve hysteresis. Thus, the threshold voltage shift and mobility degradation can be discussed separately. However, parts of trapped charges are released during the transfer characteristics measurements, so the time dependence of bias-stress effects is more or less affected. In contrast, in Method II, no release of trapped charges occurs, but the separate discussion of the threshold voltage shift and mobility degradation is not possible. This is because the on-state current degradation is caused by both a shift in the threshold voltage and a reduction in the field-effect mobility. Only if the field-effect mobility is independent of carrier concentration (gate-source voltage V_{gs}) and unchanged during prolonged gate-bias application, the bias-stress time dependence of the on-state I_d can be converted into that of ΔV_{th}^{lin}, and the τ and β determined by Method II can be compared with those determined by Method I.

Most polymer-based OFETs exhibit carrier-concentration-dependent (V_{gs}-dependent) field-effect mobility due to conformational and energitic disorder in the polymeric active layers.[12−15] Thus, even if the field-effect mobility is unchanged during bias-stress application, Method II cannot be used to determine ΔV_{th}^{lin} as a function of bias-stress time. Although it remains a useful method for evaluating the operational stability of OFETs for current-driven device applications, Method I is believed to be suitable for fundamental research into the origin of operational instability and for evaluating the effects of active layers, gate dielectrics, and active layer/gate dielectric interfaces on operational stability.

In Method I, the field-effect mobility (μ^{lin}) and threshold voltage (V_{th}^{lin}) are extracted from the transfer characteristics measured in the linear regime using the following equation:

$$I_d = -\frac{\mu^{lin} W C_i}{L} V_{ds}\left(V_{gs} - V_{th}^{lin} - \frac{V_{ds}}{2}\right) \quad (2)$$

where V_{ds} is the drain-source voltage; L and W are the channel length and width, respectively; and C_i is the gate dielectric capacitance per unit area. When the μ^{lin} is carrier-concentration-dependent, the transfer curve is not a straight line (not ideal) in the on-state V_{gs} region. Thus, for polymer-based OFETs, great care must be taken in applying eq 2. If the carrier-concentration-dependent μ^{lin} does not change during bias-stress application; that is, the V_{gs}-dependent mobility shifts by ΔV_{th}^{lin} with no change in magnitude and shape in the on-state V_{gs} region, ΔV_{th}^{lin} can be easily and accurately determined by shifting the initial transfer curve so that it overlaps with the transfer curve after bias-stressing or by applying eq 2 to the portion of the transfer curve around a certain I_d in the on-state region. In this case, the obtained ΔV_{th}^{lin} is not affected by whether R_c correction is performed or not, because the relative ratio of the total contact resistance R_c at source and drain electrodes to the channel resistance R_{ch} does not change during bias-stress application. In contrast, when the carrier-concentration-dependent μ^{lin} changes in shape and/or in magnitude during bias-stress application, one should pay attention to R_c. For OFETs where R_c is not negligibly small against R_{ch}, the operational stability may be overestimated or underestimated without R_c correction, which is the subject of this paper.

In this study, we have investigated the effect of R_c on the evaluation of operational stability of OFETs exhibiting both a shift in V_{th}^{lin} and a reduction in μ^{lin}. Bottom-gate top-contact (BG-TC) OFETs with different L's from 50 to 500 μm were fabricated on a single device substrate using poly(didodecylquaterthiophene-*alt*-didodecylbithiazole) (PQTBTz-C12) as the active layer material. PQTBTz-C12 is a D−A copolymer exhibiting a liquid crystalline (LC) phase at an elevated temperature.[16] The bias-stress effects were evaluated by Method I. The V_{gs}-dependent R_c at different bias-stress times was determined using a modified transmission-line method (TLM), which can extract R_c with much greater accuracy compared to the conventional TLM.[17,18] After the transfer characteristics were corrected using the extracted R_c, the R_c-corrected μ^{lin} and V_{th}^{lin} were obtained. Since all PQTBTz OFETs exhibited nonlinear transfer characteristics with a maximum transconductance within the V_{gs} sweep range regardless of R_c correction, here the V_{th}^{lin} was conventionally evaluated from the portion of transfer curves around V_{gs} at which μ^{lin} becomes a maximum. As a result, we found that without R_c correction, the operational stability was overestimated for OFETs with short channels. This erroneous evaluation would become more pronounced in short-channel, high-mobility OFETs, because R_c becomes larger relative to R_{ch} with increasing μ^{lin} and decreasing L. As R_c is included in the characteristics of OFETs, R_c correction may not be necessary when evaluating the operational stability of OFETs themselves. However, our results suggest that R_c correction should be performed in the fundamental research into the origin of operational instability and in evaluating the effects of active layers, gate dielectrics, and active layer/gate dielectric interfaces on operational stability. Finally, the operational stability of PQTBTz OFETs was compared to that of poly(2,5-bis(3-hexadecylthiophen-2-yl)thieno[3,2-*b*]thiophene) (PBTTT-C16) and PCDTPT OFETs evaluated in our previous work.[19,20]

2. EXPERIMENTAL SECTION

2.1. Materials. The synthesis of PQTBTz-C12 was outsourced to TCI Co. Ltd. and was carried out through the same route described in ref 16. However, the details of reaction conditions were modified, and the reaction using H_2S gas and dimethylamine in ref 16 was replaced with a reaction using NaSH and $MgCl_2$, based on ref 21. The number-average molecular weight (polystyrene standard) and polydispersity of PQTBTz-C12 used in this study were 24 kg mol^{-1} and 2.9, respectively. The differential molecular weight distribution is shown in Figure S1. It was confirmed by differential scanning calorimetry

https://doi.org/10.1021/acsami.4c15666
ACS Appl. Mater. Interfaces 2024, 16, 68081−68090

(DSC) that the polymer exhibited an LC phase between 145 and 193 °C during the heating scan. The DSC curve is presented in Figure S2. In the fabrication of OFETs, anhydrous chlorobenzene (CB) purchased from Sigma-Aldrich, electronics grade acetone and 2-propanol purchased from Kishida Chemical, toluene, dehydrated toluene, and electronics grade sulfuric acid and hydrogen peroxide purchased from Kanto Chemical, and octadecyltrichlorosilane (ODTS) provided by Acros Organics were used as received.

2.2. Fabrication of PQTBTz OFET Arrays. PQTBTz OFET arrays were fabricated on heavily doped n-type Si(100) substrates (20 × 20 mm^2) with a thermally grown SiO_2 layer (≈100 nm thick). The substrates were cleaned sequentially with acetone and a piranha solution (a mixture of sulfuric acid and hydrogen peroxide) and immediately treated with ODTS vapor at 120 °C for 3 h. The detailed procedures of the cleaning and ODTS treatment were described elsewhere.[20,22] (In this study, the nanogroove formation in ref 20 and the rubbing treatment before spin-coating in ref 22 were skipped.) The ODTS treatment was performed to minimize charge trapping at the active layer/SiO_2 gate dielectric interface. The resultant ODTS-treated surfaces showed water contact angles in excess of 110°. Spin-coating such highly hydrophobic gate dielectric surfaces with semiconducting polymer films was difficult due to the repellent nature against organic solvents (lyophobicity). This difficulty was solved by forming an appropriate hydrophobic−hydrophilic (lyophobic-lyophilic) pattern on the highly hydrophobic gate dielectric surface, and OFETs were fabricated in the hydrophobic areas.[19,20,22−24] For solution of PQTBTz-C12 in CB, a simple pattern of a 15 mm-square hydrophobic region with a 2.5 mm wide hydrophilic outer edge[24] was sufficient. This hydrophobic−hydrophilic surface pattern was produced by exposing the ODTS-treated surfaces to vacuum ultraviolet (VUV) light (wavelength 172 nm) through a photomask, as described elsewhere.[22] The VUV-light-exposed areas became hydrophilic (lyophilic). Then, 26 (37) nm-thick active layers were deposited on the substrates by spin-coating with a hot 0.40 (0.56) wt % solution of PQTBTz-C12 in CB at room temperature (RT) in air. The solution temperature was 60 °C. The rotation speed and duration of spin-coating were 1000 rpm and 180 s, respectively. Then, the spin-coated films were annealed at 180 °C for 1 h in a nitrogen atmosphere.[16] The crystallinity enhancement of perfectly oriented crystalline lamella with a *d*-spacing of 2.1 nm (edge-on molecular orientation) during annealing at 180 °C was confirmed by the out-of-plane and rocking scan X-ray diffraction (XRD) measurements.[16] The XRD profiles are shown in Figure S3. The monolayer molecular steps were confirmed in the AFM images shown in Figure S4. The PQTBTz-C12 thickness was estimated with a stylus type step profiler (Kosaka ET200).

The n^+-Si substrate and ODTS-treated SiO_2 layer served as a common gate electrode and gate dielectrics of OFETs, respectively. To complete BG-TC OFET arrays, source and drain (S/D) electrodes were formed on the annealed PQTBTz-C12 films by sequential thermal evaporation of MoO_3 (25 nm thick) and Au (40 nm thick) through a shadow mask in vacuum (base pressure <3 × 10^{-5} Pa). The thicknesses of the S/D electrodes were the reading of a thickness monitor, which was precalibrated to match the film thickness measured by a stylus type step profiler. Two different shadow masks were utilized. One was for producing 12 × 5 arrays of OFETs with L/W of 50/300 μm shown in Figure 1a. The channel directions of neighboring OFETs were orthogonal to each other. This array pattern was used to evaluate the spatial uniformity of the spin-coated PQTBTz-C12 film in terms of OFET properties. The other was for producing sets of OFETs with different L's from 50 to 500 μm in 50 μm intervals and a constant W of 500 μm shown in Figure 1b. Bias-stress measurements were performed on the sets of OFETs, and the V_{gs}-dependent R_c at different bias-stress times were extracted from their transfer characteristics. The regions enclosed by dotted lines in Figure 1 are the hydrophobic SiO_2 surface areas.

2.3. Electrical Characterization. The electrical characteristics of OFETs were measured using a vacuum probe station and a semiconductor parameter analyzer system.[19] Each OFET was electrically isolated by removing the surrounding PQTBTz-C12 film with a tungsten needle in air. Then, an OFET substrate was set in the vacuum probe station. To remove residual oxygen and moisture in the active layer, the array was annealed at 180 °C for 15 min in vacuum. First, the initial output and transfer characteristics of all OFETs were measured in the saturation regime. Then, the on-state bias-stress effects were measured by Method I for selected sets of OFETs with different L's and a constant W of 500 μm. The electrical measurement conditions will be described with the experimental data. All the above electrical measurements were performed at RT under vacuum conditions less than 10^{-4} Pa in the dark. The gate dielectric capacitance was measured with an LCR meter (HIOKI 3522−50). The C_i for all OFETs reported in this paper was 31.9 nF cm^{-2}.

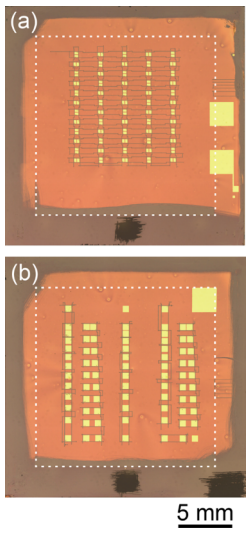

Figure 1. Optical microscope images of OFET arrays with different S/D electrode patterns. (a) 12 × 5 array of OFETs with L/W of 50/300 μm. (b) Array of OFETs with different L's and a constant W of 500 μm. The regions enclosed by the dotted lines are the hydrophobic SiO_2 surface areas.

2.4. Other Characterization. The molecular weight and thermal behavior of PQTBTz-C12 were examined with a gel permeation chromatography system (Shimadzu Nexera 40) and a differential scanning calorimeter (Shimadzu DSC-60), respectively. The contact angle measurements and optical microscope observations were performed using a Kyowa DM 500 contact angle meter and an Olympus BX51 optical microscope, respectively. The AFM images were acquired with a system composed of Hitachi High-Tech AFM5100N and AFM5000II. The out-of-plane and rocking scan XRD measurements were performed using an RIGAKU SmartLab X-ray diffractometer.

3. RESULTS AND DISCUSSION

3.1. Spatial Uniformity of PQTBTz Films from a Viewpoint of OFET Characteristics. The spatial uniformity of PQTBTz-C12 films formed on ODTS-treated SiO_2/Si substrates is crucial for extraction of reliable V_{gs}-dependent R_c by a modified TLM, because a set of OFETs with different lengths of channels with nearly identical electrical properties should be prepared. Thus, first the spatial uniformity was confirmed from the viewpoint of OFET properties. For this purpose, a 26 nm-thick PQTBTz OFET array with the S/D electrode pattern (L/W = 50/300 μm) shown in Figure1a was fabricated, and the initial electrical properties of all OFETs were measured in the saturation regime. The typical output and transfer characteristics are shown in Figure 2. The output (transfer) characteristics were acquired by negatively increasing V_{ds} (V_{gs}) down to −30 V as a forward sweep and immediately executing the reverse voltage sweep. In the output

https://doi.org/10.1021/acsami.4c15666
ACS Appl. Mater. Interfaces 2024, 16, 68081−68090

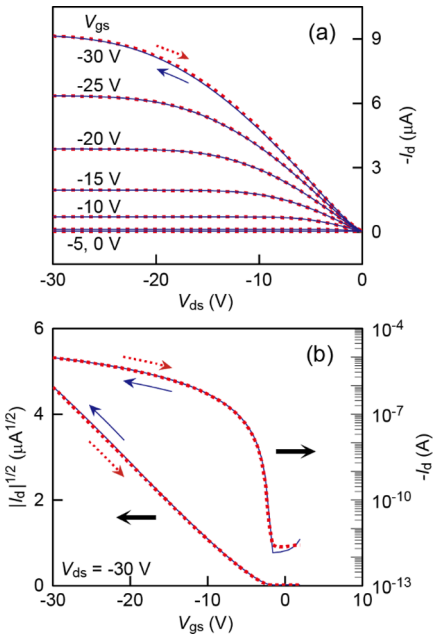

Figure 2. Typical (a) output and (b) transfer characteristics in the saturation regime of OFETs with L/W = 50/300 μm. The solid and dotted curves show the data for forward and reverse sweeps, respectively.

characteristic measurement, the V_{gs} was varied from 0 to −30 V in increments of −5 V, and in the transfer characteristic measurement, a constant V_{ds} of −30 V was applied. All OFETs showed good p-channel transistor behavior with almost no hysteresis in I_d between the forward and reverse sweeps and maximum current on/off ratios greater than 10^6. In the output characteristics, the nonlinear increase of I_d was observed in the low V_{ds} range (linear regime), which indicates that R_c is not negligible relative to R_{ch} for OFETs with L = 50 μm.

The field-effect hole mobility μ, threshold voltage V_{th}, and subthreshold swing SS were evaluated from the forward sweep transfer curves. The μ and V_{th} were extracted using the following equation describing I_d in the saturation regime:

$$|I_d| = \frac{W}{2L} C_i \mu (V_{gs} - V_{th})^2 \quad (3)$$

The SS was determined from the partial transfer curves (not shown) remeasured in intervals of 0.05 V over the turn-on V_{gs} range. The histograms of μ, V_{th}, and SS are shown in Figures 3, S5a, and S5b, respectively. The average values (A_v) and standard deviations (σ) of μ, V_{th}, and SS were 0.159 ± 0.059 cm^2 V^{-1} s^{-1}, −4.39 ± 0.23 V, and 0.265 ± 0.033 V/decade, respectively. The relative standard deviation (σ/A_v) of μ was less than 4%. In addition to μ, the device-to-device variations of V_{th} and SS were also found to be very small. From these very small device-to-device variations, it was confirmed that the uniformity of the PQTBTz-C12 films formed in this study was very high. To visually indicate the very small device-to-device variations, that is, the high spatial uniformity, the transfer curves of all 60 OFETs are plotted in Figure S6. For ease of viewing, only the transfer curves in the forward sweeps were plotted. One can see their excellent overlapping.

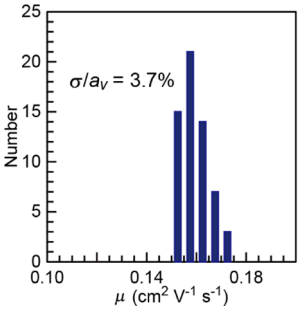

Figure 3. Histogram analysis of initial μ in the saturation regime of PQTBTz OFET arrays. The bin widths are 0.005 cm^2 V^{-1} s^{-1}.

3.2. Bias-Stress Effects of OFETs with Different Channel Lengths. The contact resistance R_c of BG-TC OFETs consists of the metal−semiconductor interface resistance R_i and the access resistance R_a from the metal−semiconductor interface to the conduction channel: that is, $R_c = R_i + R_a$. Since R_a increases with increasing active layer thickness, OFETs with different R_c can be prepared by varying the active layer thickness. To clearly demonstrate the influence of R_c on the bias-stress effect evaluation, OFET arrays with 26 and 37 nm-thick PQTBTz active layers and the S/D electrode pattern shown in Figure1b were fabricated. The bias-stress effect measurements were performed on each set of OFETs with different L's ranging from 50 to 500 μm at 50 μm intervals. As already stated, the bias-stress effects were evaluated by Method I. The bias-stress condition and measurement sequence were the same as in our previous work,[19,20] except for the V_{gs} sweep range and interval in the transfer curve measurements. In the present study, the transfer curves in the linear regime were acquired by sweeping V_{gs} between +2 and −30 V with 0.1 V intervals in the forward and reverse directions sequentially under V_{ds} = −1 V. The specific measurement sequence was as follows. A constant prolonged on-state bias-stress (V_{gs} = −30 V and V_{ds} = −1 V) was applied 1 h after completing the initial transfer curve measurement (bias-stress time of 0 s). At bias-stress times of 5 × 10^2, 5 × 10^3, and 2.5 × 10^4 s, the on-state bias-stress application was interrupted and immediately the transfer characteristics were measured, after which the on-state bias-stress was immediately reapplied, except for a bias-stress time of 2.5 × 10^4 s.

The transfer curves of 26 nm-thick PQTBTz OFETs with L = 50 and 500 μm recorded at different bias-stress times are shown by the solid and broken curves, respectively, in Figure 4a. Both OFETs exhibited nonlinear (nonideal) transfer characteristics with a maximum transconductance (g_m = dI_d/dV_{gs}) within the V_{gs} sweep range. The V_{gs}-dependent μ^{lin} (=−g_m × L/WC_iV_{ds}) calculated from the nonlinear transfer characteristics is shown in Figure 4b. For both OFETs, obvious bias-stress effects were observed in both V_{th}^{lin} and μ^{lin}; that is, the transfer curves shifted in the negative voltage direction with increasing bias-stress time and the maximum μ^{lin} gradually decreased. Here, note that the vertical axis of Figure 4a is normalized by L and W: that is, $-I_d \times L/W$. On this scale, the transfer curves in the linear regime of OFETs with different L's and W's should overlap each other when R_c is negligibly small relative to R_{ch}, as seen from eq 2. However, $|I_d| \times L/W$ at V_{gs} = −30 V for the OFET with L = 50 μm was reduced by roughly 45% compared to that for the OFET with L = 500 μm due to the non-negligible R_c. This result suggests that at V_{gs} = −30 V, R_c is approximately equal to R_{ch} of the OFET with L = 50 μm. Since R_{ch} increases proportionally to L, in the OFET with L = 500 μm, R_c is one-tenth of R_{ch}, and the effect of R_c is significantly reduced. Thus, the transfer characteristics and V_{gs}-

https://doi.org/10.1021/acsami.4c15666
ACS Appl. Mater. Interfaces 2024, 16, 68081−68090

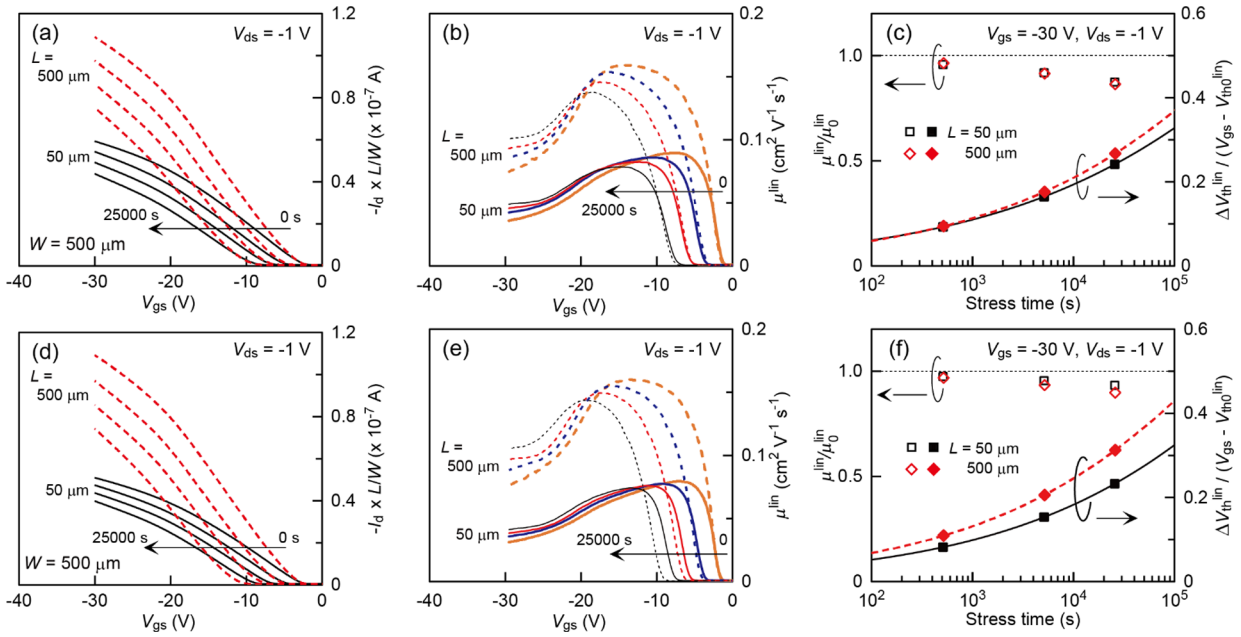

Figure 4. Bias-stress effects of PQTBTz OFETs with different active layer thicknesses of 26 (a–c) and 37 nm (d–f) and different L's of 50 (solid curves) and 500 μm (broken curves). (a,d) Transfer curves measured in the linear regime (V_{ds} = −1 V) at bias-stress times of 0, 5 × 10^2, 5 × 10^3, and 2.5 × 10^4 s. (b,e) V_{gs}-dependent μ^{lin} extracted from the transfer curves in (a,d). (c,f) Bias-stress time dependence of normalized μ^{lin} (open symbols) and ΔV_{th}^{lin} (filled symbols) for PQTBTz OFETs with L = 50 (squares) and 500 mm (diamonds). The solid and broken curves are the fitting results with eq 1a.

dependent μ^{lin} of the OFET with L = 500 μm can be considered close to the intrinsic ones without the effect of R_c. Thus, it is seen from Figure 4b that the effect of R_c not only reduces the magnitude of μ^{lin} but also significantly changes the shape of the V_{gs} dependence. The V_{gs} at which μ^{lin} is maximum shifts in the positive direction in the OFET with L = 50 μm. For OFETs exhibiting nonideal transfer characteristics, the μ^{lin} and V_{th}^{lin} are conventionally extracted from the transfer characteristics around the maximum transconductance (mobility). The shape distortion in the V_{gs} dependence of μ^{lin} due to the non-negligible R_c can lead to an erroneous evaluation of the operational stability. Figure 4c shows the bias-stress time dependence of normalized ΔV_{th}^{lin} and μ^{lin}, where the V_{th}^{lin} and μ^{lin} were extracted by the conventional way described above; and ΔV_{th}^{lin} and μ^{lin} were normalized to the initial effective bias-stress voltage ($V_{gs} - V_{th0}^{lin}$) and the initial mobility μ_0^{lin}, respectively. The μ_0^{lin} and V_{th0}^{lin}, respectively, of 26 nm-thick PQTBTz OFETs were 0.09 $cm^2 V^{-1} s^{-1}$ and −2.77 V for L = 50 μm, and 0.16 $cm^2 V^{-1} s^{-1}$ and −4.07 V for L = 500 μm. In Figure 4c, the OFET with L = 50 μm appears to be slightly stable against the prolonged bias-stress application compared to the OFET with L = 500 μm.

The corresponding data for the 37 nm-thick PQTBTz OFETs are shown in Figure 4d–f. The μ_0^{lin} and V_{th0}^{lin}, respectively, of 37 nm-thick PQTBTz OFETs were 0.08 $cm^2 V^{-1} s^{-1}$ and −2.82 V for L = 50 μm, and 0.16 $cm^2 V^{-1} s^{-1}$ and −4.00 V for L = 500 μm. As expected, the influence of R_c on the transfer characteristics and μ^{lin} can be seen more pronounced. The $|I_d| \times L/W$ at V_{gs} = −30 V was reduced by roughly half by decreasing L from 500 to 50 μm, as shown in Figure 4d. Comparing Figure 4b,e, it is seen that the reduction of μ^{lin} in decreasing L from 500 to 50 μm is larger than that for the 26 nm-thick PQTBTz OFETs. In Figure 4f, the OFET with L = 50 μm appears to be significantly more stable than the OFET with L = 500 μm. In the next section, it is demonstrated that these apparent channel length dependences in the bias-stress effects disappear after performing R_c correction on the transfer characteristics.

3.3. Contact Resistance Correction. The V_{gs}-dependent R_c at different bias-stress times was extracted in 0.1 V intervals by a modified TLM from a set of the forward-sweep transfer curves in the linear regime measured for the OFETs with different L's from 50 to 500 μm in 50 μm intervals. The channels of OFETs operating in the linear regime can be considered as an approximately uniform resistance, which is given by $R_{ch} = L/W\mu^{lin}C_i(V_{gs} - V_{th}^{lin})$. Thus, the total resistance R_{total} of OFETs is expressed by $R_{total} = R_{ch} + R_c$. These resistances are usually normalized by W to be universal for OFETs with different W's, as follows:

$$R_{total}W = \frac{L}{\mu^{lin}C_i(V_{gs} - V_{th}^{lin})} + R_cW \quad (4)$$

This is the equation used in the conventional TLM. R_cW can be obtained from the intercept to the y-axis (L = 0) in a plot of $R_{total}W$ versus L. Xu et al.[17] proposed a modified TLM as a method to determine R_cW with higher accuracy. This method is based on the equation that is obtained by dividing both sides of eq 4 by L:

$$\frac{R_{total}W}{L} = \frac{1}{\mu^{lin}C_i(V_{gs} - V_{th}^{lin})} + (R_cW)\frac{1}{L} \quad (5)$$

R_cW can be obtained from the linear regression slope in a plot of $R_{total}W/L$ versus $1/L$. For a detail discussion on the accuracy in the determination of R_cW, see ref 17.

The modified TLM plot of the 26 and 37 nm-thick PQTBTz OFETs at a bias-stress time of 0 s is shown in Figure 5a, where only data for V_{gs} = −10, −20, and −30 V are plotted for ease of viewing. The corresponding plots at bias-stress times of 5 × 10^2, 5 × 10^3, and 2.5 × 10^4 s, are presented in Figure S7. The

https://doi.org/10.1021/acsami.4c15666
ACS Appl. Mater. Interfaces 2024, 16, 68081−68090

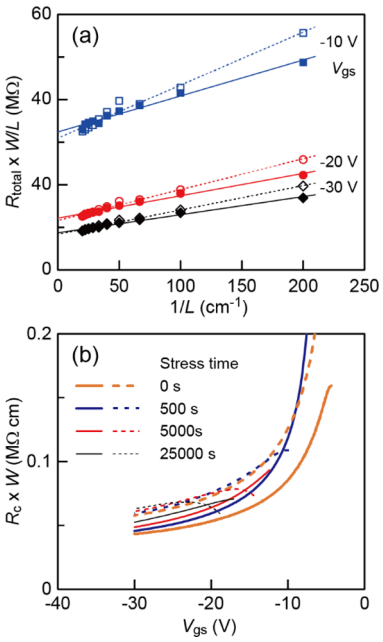

Figure 5. (a) Modified TLM plot of 26 and 37 nm-thick PQTBTz OFETs with different L's from 50 to 500 μm at a bias-stress time of 0 s; the squares, circles, and diamonds are the data points for V_{gs} = −10, −20, and −30 V, respectively. The straight lines are the regression lines. The filled and open symbols (solid and broken lines) are the data points (fitting results) for 26 and 37 nm-thick PQTBTz OFETs, respectively. (b) R_cW extracted by modified TLM at different bias-stress times. The very thick, thick, thin, and very thin curves show the results for bias-stress times of 0, 5 × 10^2, 5 × 10^3, and 2.5 × 10^4 s, respectively. The solid and broken curves are the results for 26 and 37 nm-thick PQTBTz OFETs, respectively.

filled and open symbols (solid and dotted straight lines) are the data points (regression lines) for the 26 and 37 nm-thick PQTBTz OFETs, respectively. The coefficients of determination R^2 for the 26 (37) nm-thick OFETs were 0.922 (0.976), 0.977 (0.990), and 0.985 (0.995) at V_{gs} of −10, −20, and −30 V, respectively. Since the linear regression slopes correspond to R_cW, it can be seen at a glance that the R_cW for the 37 nm-thick PQTBTz OFETs is larger than that for the 26 nm-thick PQTBTz OFETs. Figure 5b shows the V_{gs}-dependent R_cW extracted by the modified TLM. The very thick, thick, thin, and very thin curves show the results for bias-stress times of 0, 5 × 10^2, 5 × 10^3, and 2.5 × 10^4 s, respectively. The solid and broken curves are R_cW for the 26 and 37 nm-thick PQTBTz OFETs, respectively. As seen from Figure S8, when V_{gs} approached V_{th}^{lin} from the negative side, the fitting accuracy degraded rapidly. This is because in such a V_{gs} region, the contribution of $R_{ch}W$ to $R_{total}W$ becomes much larger than that of R_cW; that is, the first term on the right-hand side of eq 5 becomes dominant, making it difficult to determine the linear regression slope in the modified TLM plots with sufficient accuracy. Thus, only R_cW extracted with $R^2 \geq 0.8$ are plotted in Figure 5b and used in R_c correction. Although the unrealistic sagging of R_cW is still seen in the V_{gs}-dependence at bias-stress times of 5 × 10^2, 5 × 10^3, and 2.5 × 10^4 s for the 37 nm-thick PQTBTz OFETs, it does not significantly affect the next R_c correction.

Now, we can perform R_c correction on the transfer characteristics obtained in the bias-stress effect measurements. The R_c-corrected I_d was calculated by multiplying I_d by a R_c-correction factor F, which is given by $F = (R_{ch} + R_c)/R_{ch} = R_{total}/(R_{total} - R_c)$, where $R_{total} = V_{ds}/I_d$. The R_c-corrected transfer curves and μ^{lin} are shown in Figure 6a,d and b,e, respectively. The bias-stress time dependence of $\Delta V_{th}^{lin}/(V_{gs} - V_{th0}^{lin})$ and μ^{lin}/μ_0^{lin} evaluated from the R_c-corrected transfer

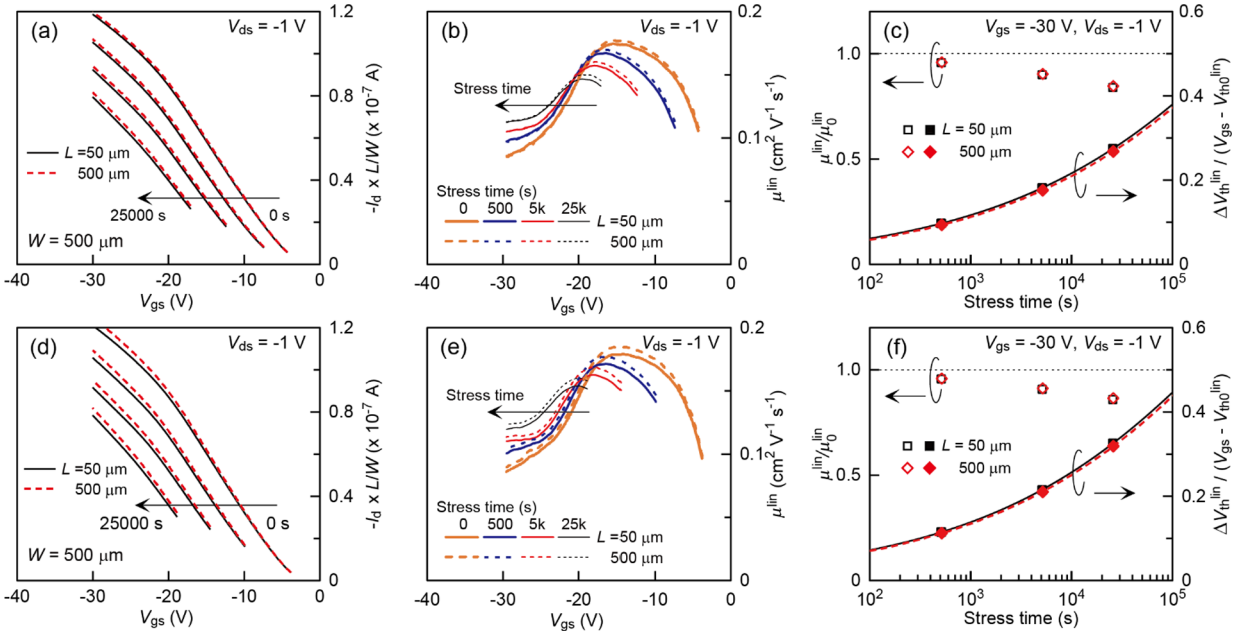

Figure 6. Bias-stress effects of PQTBTz OFETs with different active layer thicknesses of 26 (a−c) and 37 nm (d−f) and different L's of 50 (solid curves) and 500 μm (broken curves) after R_c correction. (a,d) R_c-corrected transfer curves in the linear regime (V_{ds} = −1 V) at bias-stress times of 0, 5 × 10^2, 5 × 10^3, and 2.5 × 10^4 s. (b,e) R_c-corrected V_{gs}-dependent μ^{lin} extracted from the transfer curves in (a,d). (c,f) R_c-corrected bias-stress time dependence of normalized μ^{lin} (open symbols) and ΔV_{th}^{lin} (filled symbols) for PQTBTz OFETs with L = 50 (squares) and 500 μm (diamonds). The solid and broken curves are the fitting results with eq 1a.

https://doi.org/10.1021/acsami.4c15666
ACS Appl. Mater. Interfaces 2024, 16, 68081−68090

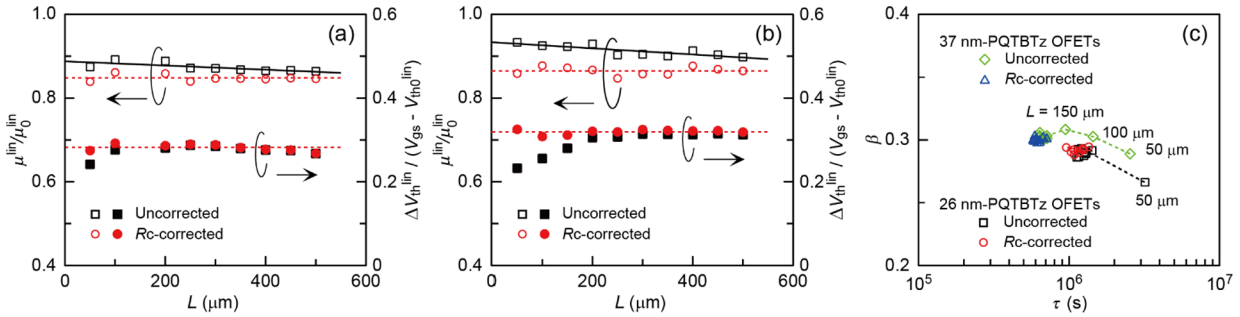

Figure 7. (a,b) μ^{lin}/μ_0^{lin} (open symbols) and $\Delta V_{th}^{lin}/(V_{gs} - V_{th0}^{lin})$ (filled symbols) without (squares) and with (circles) R_c correction at a bias-stress time of 2.5×10^4 s as a function of L: (a) 26 nm-thick PQTBTz OFETs and (b) 37 nm-thick PQTBTz OFETs. (c) τ and β determined for 26 nm- (squares and circles) and 37 nm- (diamonds and triangles) PQTBTz OFETs with different L's. Circles and triangles (squares and diamonds) are data with (without) R_c correction.

curves are shown in Figure 6c,f, where the R_c-corrected μ_0^{lin} and V_{th0}^{lin}, respectively, of 26 (37) nm-thick PQTBTz OFETs were 0.17 (0.18) $cm^2 V^{-1} s^{-1}$ and −4.48 (−4.39) V for L = 50 μm and 0.18 (0.18) $cm^2 V^{-1} s^{-1}$ and −4.45 (−4.43) V for L = 500 μm. From these figures, it was found that the channel length dependence seen in Figure 4 disappeared after R_c correction. Therefore, the apparent higher operational stability of the OFETs with L = 50 μm compared to that of the OFETs with L = 500 μm in Figure 4c,f was due to the effect of a non-negligible R_c.

Figure 7a,b shows the channel length dependence of $\Delta V_{th}^{lin}/(V_{gs} - V_{th0}^{lin})$ and μ^{lin}/μ_0^{lin} at a bias-stress time of 2.5×10^4 s before (squares) and after (circles) R_c correction for the 26 and 37 nm-thick PQTBTz OFETs, respectively. The solid lines in these figures are guides to the eye, and the dotted lines show the average values for the OFETs with L's from 50 to 500 μm. Both $\Delta V_{th}^{lin}/(V_{gs} - V_{th0}^{lin})$ and μ^{lin}/μ_0^{lin} are seen to be constant independent of L after R_c correction. The influence of R_c can be seen more clearly in Figure 7b. Before R_c correction, the reduction in μ^{lin} caused by bias-stress application increases with increasing L but it is still underestimated even at L = 500 μm compared to that after R_c correction. On the other hand, $\Delta V_{th}^{lin}/(V_{gs} - V_{th0}^{lin})$ increases with increasing L up to 200 μm, then being constant and almost equal to the average value of the R_c-corrected $\Delta V_{th}^{lin}/(V_{gs} - V_{th0}^{lin})$. The similar trend can be seen in Figure 7a. From these figures, we found that without R_c correction, the reduction of μ^{lin} was underestimated even for the OFETs with L = 500 μm, and ΔV_{th}^{lin} was underestimated in the OFETs with short channels: ≤50 (150) μm for the 26 (37) nm-thick active layers. That is, the operational stability was found to be overestimated without R_c correction.

The fitting of the bias-stress time dependence of $\Delta V_{th}^{lin}/(V_{gs} - V_{th0}^{lin})$ before and after R_c correction with eq 1a was performed for both sets of the OFETs with different L's. The obtained τ and β were plotted as a function of L in Figure S9 and as τ–β mapping in Figure 7c. These figures explicitly show that the channel length dependence disappears after R_c correction, which indicates the reliability of R_c correction performed in this study. Therefore, we successfully evaluated the bias-stress effect in BG-TC PQTBTz OFETs with an ODTS-treated SiO_2 gate dielectric excluding the influence of R_c. The average values of R_c-corrected τ and β for the 26 (37) nm-thick PQTBTz OFETs were 1.2 (0.6) × 10^6 s and 0.29 (0.30), respectively, and the R_c-corrected μ^{lin}/μ_0^{lin} was on average 0.85 (0.86) at 2.5×10^4 s. Figures 7 and S9 suggest a simple and effective way to avoid erroneous estimation in τ, β, and ΔV_{th}^{lin}, when a set of OFETs with different L's cannot be prepared in sufficient intervals to determine R_cW by the modified TLM; it is to evaluate the bias-stress effect on two OFETs whose channel lengths differ by more than a factor of 2 and ensure that they are equal within the experimental uncertainty. Before closing this subsection, we would like to note that the erroneous evaluation of the operational stability would become more pronounced in short-channel, high-mobility OFETs, because R_c becomes larger relative to R_{ch} with increasing μ^{lin} and decreasing L.

3.4. Comparison of Operational Stability among PBTTT, PCDTPT, and PQTBTz OFETs. In our previous work,[19,20] the operational stability of BG-TC OFETs with 24 nm-thick PBTTT-C16 and 16 nm-thick PCDTPT active layers formed on ODTS-treated SiO_2 (≈100 nm thick)/Si substrates was evaluated under vacuum environment. Since extrinsic factors such as the atmospheric oxygen and moisture affect the operational stability of OFETs, burying the intrinsic relationship between the operational stability and the properties of constituent materials, the evaluation under vacuum environment is essential to investigate the origin of intrinsic operational instability. Interestingly, these two OFETs showed only a shift in V_{th}^{lin} with almost no change in the carrier-concentration-dependent μ^{lin}, as shown in Figure S10. As explained in Introduction, R_c correction is no need for these OFETs.

In the present study, the operational stability of PQTBTz OFETs in a vacuum environment was evaluated under the same bias-stress condition and measurement sequence as in the previous work.[19,20] The device structure of the 26 nm-thick PQTBTz OFETs with L/W = 50/500 μm was almost the same as those of the PBTTT and PCDTPT OFETs. Thus, the operational stability among the three OFETs can be compared with minimum uncertainty, allowing us to discuss the origin causing the difference in operational stability. This comparison is also interesting from the perspective of the difference in thermal behavior of semiconducting polymers; PBTTT-C16 and PQTBTz-C12 exhibit LC phases at elevated temperatures, whereas PCDTPT reveals no LC phase up to 300 °C.[25] For PBTTT[26] and PQTBTz, the active layers consisting of perfectly oriented crystalline lamellae throughout the entire film thickness are formed by annealing at the LC temperature (150 and 180 °C, respectively). For PCDTPT, the formation of perfectly oriented crystalline lamellae is confined to less than 10 nm near the ODTS-treated SiO_2 gate insulator surfaces, even after annealing at 200 °C.[19] The difference in thermal behavior appeared as that in the surface morphology; wide

https://doi.org/10.1021/acsami.4c15666
ACS Appl. Mater. Interfaces 2024, 16, 68081−68090

Table 1. Summary of $\Delta V_{th}^{lin}/(V_{gs} - V_{th0}^{lin})$ at 2.5×10^4 s, τ, and β of OFETs with PQTBTz, PCDTPT, and PBTTT Active Layers[a]

semiconductor (thickness)	gate-dielectric (L/W of OFET)	$\frac{\Delta V_{th}^{lin}}{(V_{gs} - V_{th0}^{lin})}$ at 25k s	τ [s]	β	atmosphere	ref
PQTBTz (26 nm)	ODTS-SiO_2 (50/500 μm)	0.27	1×10^6	0.29	in vac.	this work
PCDTPT (16 nm)	ODTS-SiO_2 (50/300 μm)	0.24	1×10^6	0.32	in vac.	19
pBTTT-C16 (24 nm)	ODTS-SiO_2 (50/300 μm)	0.08	3×10^8	0.26	in vac.	19,20

[a]Thickness of SiO_2 is approximately 100 nm for all OFETs.

terraces with the single monolayer step height could be seen only for the PBTTT and PQTBTz active layers as shown in Figure S11.

To compare the operational stability of the PQTBTz, PBTTT and PCDTPT OFETs, their $\Delta V_{th}^{lin}/(V_{gs} - V_{th0}^{lin})$ at a bias-stress time of 2.5×10^4 s, τ and β are summarized in Table 1. A smaller $\Delta V_{th}^{lin}/(V_{gs} - V_{th0}^{lin})$ and a longer τ (if β is the same) indicate higher stability in V_{th}^{lin}. In addition to ΔV_{th}^{lin}, the reduction in μ^{lin} should be considered in the evaluation of operational stability. The PBTTT and PCDTPT OFETs exhibited no reduction in μ^{lin} in contrast to the PQTBTz OFETs. Therefore, the operational stability was found to be higher in the following order: PBTTT $\gg$ PCDTPT > PQTBTz.

The V_{th}^{lin} is considered the sum of the flat-band voltage (V_{FB}) of the active layer and the V_{th}^{lin} component (V_{deep}) originating in the charge carriers trapped in deep interface trapping sites.[19] The V_{deep} is given by $V_{deep} = -Q_{deep}/C_i$, where Q_{deep} is the immobilized charge carrier density. Assuming that the V_{FB} is equal to the turn-on voltage (V_{on}) in the transfer characteristics in the linear regime,[27,28] the V_{deep} can be evaluated by $V_{th}^{lin} - V_{on}$, as shown in Figure S12. To understand the origin of the difference in operational stability among the PBTTT, PCDTPT, and PQTBTz OFETs, their ΔV_{th}^{lin}, ΔV_{FB}, and ΔV_{deep} at a bias-stress time of 2.5×10^4 s are plotted in Figure 8. Interestingly, there was almost no

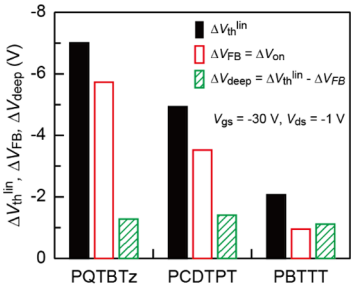

Figure 8. ΔV_{th}^{lin}, ΔV_{FB}, and ΔV_{deep} at a bias-stress time of 2.5×10^4 s for the PQTBTz, PCDTPT, and PBTTT OFETs.

difference in ΔV_{deep} among the three OFETs. The difference in the operational stability was found to come mainly from ΔV_{FB}. The $|\Delta V_{FB}|$ of the PQTBTz and PCDTPT OFETs was about 6 and 4 times larger than that of the PBTTT OFETs, respectively.

The negative ΔV_{FB} means an increase in the downward band bending near the gate dielectric/active layer interface. The most likely mechanism causing ΔV_{FB} in a vacuum environment is the charge carrier transfer from the channel to the gate dielectric under on-state gate-bias application.[29,30] For p-channel OFETs, the HOMO level mismatch between the active layer and gate dielectric (surface) acts as an energy barrier to limit the charge carrier (hole) transfer from the channel to the localized HOMO states of the gate dielectric (surface). Since the gate dielectrics of the PBTTT, PCDTPT, and PQTBTz OFETs are the same: ODTS-treated 100 nm-thick SiO_2 layers, the HOMO level mismatch decreases as the ionization potential (IP) of active layer increases. That is, the transfer rate of charge carriers increases with increasing IP of the active layer, reducing the operational stability. The IPs of PBTTT-C14, PCDTPT, and PQTBTz-C12 were reported to be 4.7–4.8,[31–33] 5.16,[25] and 5.19 eV,[16] respectively. Although the comparison of IPs reported by different research groups involves uncertainty, we believe that the trend in the magnitude of IP is as follows: PBTTT < PCDTPT $\leq$ PQTBTz. This is consistent with the trend in the $|\Delta V_{FB}|$ shown in Figure 8. Therefore, the difference in the operational stability among the three OFETs can be explained by the charge carrier transfer from the channel to the gate dielectric. This conclusion is in line with that in our previous study,[19] in which the charge carrier transfer was discussed in detail as the most likely mechanism causing ΔV_{FB}. To avoid repetition, we will not discuss it further.

Finally, we would like to note that the formation of active layers through LC phases does not necessarily lead to high operational stability. Forming the active layers through the LC phase is expected to improve the molecular packing in the π-stacking direction within the perfectly oriented crystalline lamellas, increasing the resistivity of confirmational change against the prolong gate-bias stress application. This should suppress the generation of both shallow and deep interface trapping sites. Unexpectedly, no significant difference in ΔV_{deep} was observed among the three OFETs. Moreover, a decrease in μ^{lin}, indicating the increase in shallow trap density,[34] was observed only in the PQTBTz OFETs. Therefore, the superiority of active layer formation through the LC phase in improving the operational stability was not confirmed in this study.

4. CONCLUSIONS

The operational stability of polymer-based OFETs exhibiting both a shift in V_{th}^{lin} and a reduction in μ^{lin} has been investigated. BG-TC PQTBTz OFETs with different L's from 50 to 500 μm in 50 μm intervals were fabricated on ODTS-treated SiO_2 (100 nm thick)/Si substrates and their bias-stress effects were evaluated. The ΔV_{th}^{lin} and μ^{lin}/μ_0^{lin} caused by a prolonged on-state gate-bias apprication depended on L; the $|\Delta V_{th}^{lin}|$ and the reduction in μ^{lin} increased with increasing L. Apparently, this result indicates that the OFET with a shorter L is more stable against the on-state gate-bias application. After R_c correction was performed on the transfer characteristics, the apparent channel length dependence disappeared. The reduction in μ^{lin} before R_c correction was smaller than that after, regardless of L. Without R_c correction, the $|\Delta V_{th}^{lin}|$ was underestimated in the OFETs with short channels, in which R_c was non-negligible relative to R_{ch}. That is, the operational

https://doi.org/10.1021/acsami.4c15666
ACS Appl. Mater. Interfaces 2024, 16, 68081–68090

stability was found to be overestimated for short-channel OFETs without R_c correction. As R_c becomes larger relative to R_{ch} with increasing μ^{lin} and decreasing L, the erroneous evaluation of the operational stability would become more pronounced in short-channel, high-mobility OFETs. Therefore, one should pay attention to R_c in the fundamental research into the origin of operational instability and in evaluating the effects of active layers, gate dielectrics, and active layer/gate dielectric interfaces on operational stability. Finally, the operational stability of the PQTBTz OFETs in a vacuum environment was compared to that of PCDTPT and PBTTT OFETs reported in our previous work. The operational stability was found to be higher in the following order: PBTTT ≫ PCDTPT > PQTBTz. The difference in the operational stability among the three OFETs came from the difference in ΔV_{FB}. This can be explained by the charge carrier transfer from the channel to the gate dielectric during on-state gate-bias application.

■ ASSOCIATED CONTENT

Supporting Information

The Supporting Information is available free of charge at https://pubs.acs.org/doi/10.1021/acsami.4c15666.

Additional figures as mentioned in the text, including differential molecular weight distribution and a DSC curve of PQTBTz-C12; XRD profiles and AFM images of PQTBTz-C12 films; histogram analysis of V_{th} and SS; overlaid transfer curves of 60 OFETs; modified TLM plots; extracted R_cW with R^2; channel length dependence of τ and β; bias-stress effects of PBTTT and PCDTPT OFETs; AFM images of PBTTT, PCDTPT, and PQTBTz active layers; and relationship among V_{FB} (V_{on}), V_{deep}, and V_{th}^{lin} (PDF)

■ AUTHOR INFORMATION

Corresponding Author

Kenji Sakamoto − *Research Center for Macromolecules and Biomaterials, National Institute for Materials Science (NIMS), Tsukuba, Ibaraki 305-0044, Japan;* orcid.org/0000-0002-1379-874X; Email: SAKAMOTO.Kenji@nims.go.jp

Authors

Takeshi Yasuda − *Research Center for Macromolecules and Biomaterials, National Institute for Materials Science (NIMS), Tsukuba, Ibaraki 305-0047, Japan;* orcid.org/0000-0003-4652-9105

Takeo Minari − *Research Center for Macromolecules and Biomaterials, National Institute for Materials Science (NIMS), Tsukuba, Ibaraki 305-0044, Japan;* orcid.org/0000-0001-7690-221X

Masafumi Yoshio − *Research Center for Macromolecules and Biomaterials, National Institute for Materials Science (NIMS), Tsukuba, Ibaraki 305-0047, Japan;* orcid.org/0000-0002-1442-4352

Junpei Kuwabara − *Tsukuba Research Center for Energy Materials Science (TREMS), Institute of Pure and Applied Sciences, University of Tsukuba, Tsukuba, Ibaraki 305-8573, Japan;* orcid.org/0000-0002-9032-5655

Masayuki Takeuchi − *Research Center for Macromolecules and Biomaterials, National Institute for Materials Science (NIMS), Tsukuba, Ibaraki 305-0047, Japan;* orcid.org/0000-0002-0207-0665

Complete contact information is available at: https://pubs.acs.org/10.1021/acsami.4c15666

Author Contributions

The manuscript was written through contributions of all authors. All authors have given approval to the final version of the manuscript.

Notes

The authors declare no competing financial interest.

■ ACKNOWLEDGMENTS

A part of this work was supported by JSPS KAKENHI Grant No. 20K05310 and by "Advanced Research Infrastructure for Materials and Nanotechnology in Japan (ARIM)" of the Ministry of Education, Culture, Sports, Science and Technology (MEXT), Proposal Number JPMXP1223NM5185.

■ REFERENCES

(1) Tsumura, A.; Koezuka, H.; Ando, T. Macromolecular electronic device: Field-effect transistor with a polythiophene thin film. *Appl. Phys. Lett.* **1986**, *49*, 1210−1212.

(2) Dong, H.; Fu, X.; Liu, J.; Wang, Z.; Hu, W. 25th Anniversary Article: Key Points for High-Mobility Organic Field-Effect Transistors. *Adv. Mater.* **2013**, *25*, 6158−6183.

(3) Yamashita, Y.; Hinkel, F.; Marszalek, T.; Zajaczkowski, W.; Pisula, W.; Baumgarten, M.; Matsui, H.; Müllen, K.; Takeya, J. Mobility Exceeding 10 cm^2 /(V·s) in Donor-Acceptor Polymer Transistors with Band-like Charge Transport. *Chem. Mater.* **2016**, *28*, 420−424.

(4) Luo, C.; Kyaw, A. K. K.; Perez, L. A.; Patel, S.; Wang, M.; Grimm, B.; Bazan, G. C.; Kramer, E. J.; Heeger, A. J. General Strategy for Self-Assembly of Highly Oriented Nanocrystalline Semiconducting Polymers with High Mobility. *Nano Lett.* **2014**, *14*, 2764−2771.

(5) Park, Y.; Jung, J. W.; Kang, H.; Seth, J.; Kang, Y.; Sung, M. M. Single-Crystal Poly[4-(4,4-dihexadecyl-4H-cyclopenta[1,2-b:5,4-b′]-dithiophen-2-yl)-alt-[1,2,5]thiadiazolo[3,4-c]pyridine] Nanowires with Ultrahigh Mobility. *Nano Lett.* **2019**, *19*, 1028−1032.

(6) Bittle, E. G.; Basham, J. I.; Jackson, T. N.; Jurchescu, O. D.; Gundlach, D. J. Mobility overestimation due to gated contacts in organic field-effect transistors. *Nat. Commun.* **2016**, *7*, No. 10908.

(7) Okachi, T. Mobility overestimation due to minority carrier injection and trapping in organic field-effect transistors. *Org. Electron.* **2018**, *57*, 34−44.

(8) Sirringhaus, H. Reliability of Organic Field-Effect Transistors. *Adv. Mater.* **2009**, *21*, 3859−3873.

(9) Park, S.; Kim, S. H.; Choi, H. H.; Kang, B.; Cho, K. Recent Advances in the Bias Stress Stability of Organic Transistors. *Adv. Funct. Mater.* **2020**, *30*, No. 1904590.

(10) Lee, W. H.; Choi, H. H.; Kim, D. H.; Cho, K. 25th Anniversary Article: Microstructure Dependent Bias Stability of Organic Transistors. *Adv. Mater.* **2014**, *26*, 1660−1680.

(11) Kunii, M.; Iino, H.; Hanna, J. Bias-Stress Characterization of Solution-Processed Organic Field-Effect Transistor Based on Highly Ordered Liquid Crystals. *Appl. Phys. Lett.* **2017**, *110*, No. 243301.

(12) Noriega, R.; Rivnay, J.; Vandewal, K.; Koch, F. P. V.; Stingelin, N.; Smith, P.; Toney, M. F.; Salleo, A. A general relationship between disorder, aggregation and charge transport in conjugated polymers. *Nat. Mater.* **2013**, *12*, 1038−1044.

(13) Mathijssen, S. G. J.; Cölle, M.; Gomes, H.; Smits, E. C. P.; de Boer, B.; McCulloch, I.; Bobbert, P. A.; de Leeuw, D. M. Dynamics of threshold voltage shifts in organic and amorphous silicon field-effect transistors. *Adv. Mater.* **2007**, *19*, 2785−2789.

(14) Venkateshvaran, D.; Nikolka, M.; Sadhanala, A.; Lemaur, V.; Zelazny, M.; Kepa, M.; Hurhangee, M.; Kronemeijer, A. J.; Pecunia,

V.; Nasrallah, I.; Romanov, I.; Broch, K.; McCulloch, I.; Emin, D.; Olivier, Y.; Cornil, J.; Beljonne, D.; Sirringhaus, H. Approaching disorder-free transport in high-mobility conjugated polymers. *Nature* **2014**, *515*, 384−388.
(15) Liu, C.; Huang, K.; Park, W.-T.; Li, M.; Yang, T.; Liu, X.; Liang, L.; Minari, T.; Noh, Y.-Y. A unified understanding of charge transport in organic semiconductors: the importance of attenuated delocalization for the carriers. *Mater. Horiz.* **2017**, *4*, 608−618.
(16) Kim, D. H.; Lee, B.-L.; Moon, H.; Kang, H. M.; Jeong, E. J.; Park, J.-I.; Han, K.-M.; Lee, S.; Yoo, B. W.; Koo, B. W.; Kim, J. Y.; Lee, W. H.; Cho, K.; Becerril, H. A.; Bao, Z. Liquid-Crystalline Semiconducting Copolymers with Intramolecular Donor−Acceptor Building Blocks for High-Stability Polymer Transistors. *J. Am. Chem. Soc.* **2009**, *131*, 6124−6132.
(17) Xu, Y.; Gwoziecki, R.; Chartier, I.; Coppard, R.; Balestra, F.; Ghibaudo, G. Modified transmission-line method for contact resistance extraction in organic field-effect transistors. *Appl. Phys. Lett.* **2010**, *97*, No. 063302.
(18) Liu, C.; Xu, Y.; Li, Y.; Scheideler, W.; Minari, T. Critical Impact of Gate Dielectric Interfaces on the Contact Resistance of High-Performance Organic Field-Effect Transistors. *J. Phys. Chem. C* **2013**, *117*, 12337−12345.
(19) Sakamoto, K.; Bulgarevich, K.; Yasuda, T.; Minari, T.; Takeuchi, M. Origin of intrinsic operational instability in organic field-effect transistors with aligned high-mobility donor-acceptor copolymer active layers. *Adv. Mater. Technol.* **2024**, *9*, No. 2301503.
(20) Bulgarevich, K.; Sakamoto, K.; Minari, T.; Yasuda, T.; Miki, K.; Takeuchi, M. Polymer-Based Organic Field-Effect Transistors with Active Layers Aligned by Highly Hydrophobic Nanogrooved Surfaces. *Adv. Funct. Mater.* **2019**, *29*, No. 1905365.
(21) Bronstein, H.; Hurhangee, M.; Fregoso, E. C.; Beatrup, D.; Soon, Y. W.; Huang, Z.; Hadipour, A.; Tuladhar, P. S.; Rossbauer, S.; Sohn, E.-H.; Shoaee, S.; Dimitrov, S. D.; Frost, J. M.; Ashraf, R. S.; Kirchartz, T.; Watkins, S. E.; Song, K.; Anthopoulos, T.; Nelson, J.; Rand, B. P.; Durrant, J. R.; McCulloch, I. Isostructural, Deeper Highest Occupied Molecular Orbital Analogues of Poly(3-hexylthiophene) for High-Open Circuit Voltage Organic Solar Cells. *Chem. Mater.* **2013**, *25*, 4239−4249.
(22) Bulgarevich, K.; Sakamoto, K.; Minari, T.; Yasuda, T.; Miki, K. Spatially Uniform Thin-Film Formation of Polymeric Organic Semiconductors on Lyophobic Gate Insulator Surfaces by Self-Assisted Flow-Coating. *ACS Appl. Mater. Interfaces* **2017**, *9*, 6237−6245.
(23) Bulgarevich, K.; Sakamoto, K.; Yasuda, T.; Minari, T.; Takeuchi, M. Operational Stability Enhancement of Polymeric Organic Field-Effect Transistors by Amorphous Perfluoropolymers Chemically Anchored to Gate Dielectric Surfaces. *Adv. Electron. Mater.* **2020**, *6*, No. 2000161.
(24) Horii, Y.; Sakaguchi, K.; Chikamatsu, M.; Azumi, R.; Yase, K.; Kitagawa, M.; Konishi, H. High-Performance Solution-Processed n-Channel Organic Thin-Film Transistors Based on a Long Chain Alkyl-Substituted C_{60} Derivative. *Appl. Phys. Express* **2010**, *3*, No. 101601.
(25) Ying, L.; Hsu, B. B. Y.; Zhan, H.; Welch, G. C.; Zalar, P.; Perez, L. A.; Kramer, E. J.; Nguyen, T.-Q.; Heeger, A. J.; Wong, W.-Y.; Bazan, G. C. Regioregular Pyridal[2,1,3]thiadiazole π-Conjugated Copolymers. *J. Am. Chem. Soc.* **2011**, *133*, 18538−18541.
(26) Himmelberger, S.; Dacuña, J.; Rivnay, J.; Jimison, L. H.; McCarthy-Ward, T.; Heeney, M.; McCulloch, I.; Toney, M. F.; Salleo, A. Effects of Confinement on Microstructure and Charge Transport in High Performance Semicrystalline Polymer Semiconductors. *Adv. Funct. Mater.* **2013**, *23*, 2091−2098.
(27) Haneef, H. F.; Zeidell, A. M.; Jurchescu, O. D. Charge carrier traps in organic semiconductors: a review on the underlying physics and impact on electronic devices. *J. Mater. Chem. C* **2020**, *8*, 759−787.
(28) Iqbal, H. F.; Ai, Q.; Thorley, K. J.; Chen, H.; McCulloch, I.; Risko, C.; Anthony, J. E.; Jurchescu, O. D. Suppressing bias stress degradation in high performance solution processed organic transistors operating in air. *Nat. Commun.* **2021**, *12*, No. 2352.
(29) Kim, J.; Jang, J.; Kim, K.; Kim, H.; Kim, S. H.; Park, C. E. The Origin of Excellent Gate-Bias Stress Stability in Organic Field-Effect Transistors Employing Fluorinated-Polymer Gate Dielectrics. *Adv. Mater.* **2014**, *26*, 7241−7246.
(30) Lee, B.; Wan, A.; Mastrogiovanni, D.; Anthony, J. E.; Garfunkel, E.; Podzorov, V. Origin of the bias stress instability in single-crystal organic field-effect transistors. *Phys. Rev. B* **2010**, *82*, No. 085302.
(31) Zhuo, J.-M.; Zhao, L.-H.; Png, R.-Q.; Wong, L.-Y.; Chia, P.-J.; Tang, J.-C.; Sivaramakrishnan, S.; Zhou, M.; Ou, E. C. -W.; Chua, S.-J.; Sim, W.-S.; Chua, L.-L.; Ho, P. K. -H. Direct Spectroscopic Evidence for a Photodoping Mechanism in Polythiophene and Poly(bithiophene-alt-thienothiophene) Organic Semiconductor Thin Films Involving Oxygen and Sorbed Moisture. *Adv. Mater.* **2009**, *21*, 4747−4752.
(32) Zhao, L.-H.; Png, R.-Q.; Chiam, C. C. H.; Guo, H.; Zhuo, J.-M.; Chua, L.-L.; Wee, A. T. S.; Ho, P. K. H. Polarization effects on energy-level alignment at the interfaces of polymer organic semiconductor films. *Appl. Phys. Lett.* **2012**, *101*, No. 053304.
(33) Yamashita, Y.; Tsurumi, J.; Ohno, M.; Fujimoto, R.; Kumagai, S.; Kurosawa, T.; Okamoto, T.; Takeya, J.; Watanabe, S. Efficient molecular doping of polymeric semiconductors driven by anion exchange. *Nature* **2019**, *572*, 634−638.
(34) Li, C.; Duan, L.; Li, H.; Qiu, Y. Universal Trap Effect in Carrier Transport of Disordered Organic Semiconductors: Transition from Shallow Trapping to Deep Trapping. *J. Phys. Chem. C* **2014**, *118*, 10651−10660.